Analysis of a Magnetically Suspended, High-Performance Instrument Pointing System

Suresh M. Joshi*
Old Dominion University Research Foundation, Norfolk, Va.

This paper describes a highly accurate auxiliary instrument pointing system which can provide fine pointing for a variety of solar-, stellar-, and Earth-viewing scientific instruments during extended space shuttle orbital missions. This system, called the Annular Suspension and Pointing System (ASPS), consists of pointing assemblies for coarse and vernier pointing. The "coarse" assembly is attached to the spacecraft (e.g., the space shuttle) and consists of an elevation gimbal and a lateral gimbal to provide coarse pointing. The vernier pointing assembly consists of the payload instrument mounted on a plate around which is attached a continuous annular rim. The vernier assembly is suspended in the lateral gimbal using magnetic actuators which provide rim suspension forces and fine pointing torques. A detailed linearized mathematical model is developed for the ASPS/space shuttle system, and control laws and payload attitude state estimators are designed. Statistical pointing performance is predicted in the presence of stochastic disturbances such as crew motion, sensor noise, and actuator noise.

Nomenclature

A, A_{ij} = system coefficient matrices
$A_{\rm cr}$ = crew motion filter coefficient matrix
A_j = points on the payload assembly annular rim which correspond to the magnetic bearing stations on lateral coarse gimbal
A_{CF}, A'_{CF} = magnetic force coefficient matrices
a = controller coefficient (rate gain)
A, A_i = coefficient matrices
B = system input matrix
$b_{\rm cr}$ = crew motion input matrix
B_j = magnetic bearing stations on lateral coarse gimbal
b = controller coefficient (proportional gain)
$C_p(x)$ = cross-product matrix of vector x $(x \times y = C_p(x)y)$
C_{Ix}, C_{Iy}, C_{Iz} = integrator coefficients for position loop
D_{AB} = transformation matrix from A coordinate system into B coordinate system
E = angular velocity transformation matrix defined in Eq. (2)
F_j = $(F_{xj}, F_{yj}, F_{zj})^T$, magnetic forces at the jth bearing station
F_c = crew motion force vector
F_ζ = generalized forces corresponding to the subscript coordinates
F_b = bias force vector due to cable
$F_{\rm cable}$ = cable force vector
$G_\epsilon(s)$ = transfer function of position loop compensating network
g_1, g_2 = elevation and lateral coarse gimbals
$H(s)$ = crew motion filter transfer function
I = inertia matrix defined in Eq. (4) (with subscripts)
I_{xx}, I_{yy}, I_{xy}, etc. = elements of inertia matrix
J = objective function
$K_{Fxs}, K_{Fys}, K_{Fzs}$ = cable force spring constants
K_{gl}, K_{g2} = coarse gimbal rate gains
K_{Ts} = cable torsional spring constant
L_{gl}, L_{g2} = coarse gimbal proportional gains
m = $m_s + m_{gl} + m_{g2}$
m_s = mass of the shuttle
m_{gl}, m_{g2} = masses of coarse gimbals
m_p = mass of payload
n_f = order of crew motion filter state vector
P_1 = origin of the coordinate system (X_{gl}, Y_{gl}, Z_{gl})
P_2 = origin of the coordinate system (X_{g2}, Y_{g2}, Z_{g2})
Q = center of instrument mounting surface
r = radius of instrument mounting surface
T = kinetic energy
T_1, T_2, T_3 = transformation matrices for 1, 2, 3 Eulerian rotations
T_b = bias torque due to cable
$T_{\rm cable}$ = cable torque
$T_{\rm cons}$ = shuttle attitude control torque vector
u_c = white noise with unit power spectral density
v_{ABC} = linear velocity of point "A" relative to B coordinate frame, expressed along C coordinates
w_T = input white noise vector
$w_{\rm bias}$ = bias vector
x = state vector
x_b = steady-state value of x
x_c = crew motion state vector
y_ϵ = position loop compensating network output
z_{Ix}, z_{Iy}, z_{Iz} = integrator state variables
z_{p2gl} = distance between points P_1 and P_2
α_s = shuttle altitude vector
α_p, α_q = payload altitude vectors
δ = error variable
δ_j = (three-axis) centering errors at the jth magnetic bearing station
ϵ = payload assembly position error
λ = controller output
ρ = damping ratios (with subscripts)
Σ = covariance matrix of x
σ_x = standard deviation of x
τ_1, τ_2 = time constants
τ_{c1}, τ_{c2} = crew motion filter parameters
τ_{m1}, τ_{m2} = coarse gimbal driving torques
$(\phi_s, \theta_s, \psi_s)$ = components of α_s
ϕ_g = elevation coarse gimbal angle

Received May 6, 1977; revision received Sept. 6, 1977.

Index categories: Sensor Systems; Spacecraft Systems; Space Station Systems, Manned.

*Assistant Professor (Research).

$(\phi_p, \theta_p, \psi_p)$ = components of α_q
$(\phi_q, \theta_q, \psi_q)$ = components of τ_q
ϕ_I = target pointing angle
θ_g = lateral coarse gimbal angle
θ_I = target pointing angle
Ω_{g_1} = angular velocity of g_1 frame relative to s-frame
Ω_{g_2} = angular velocity of g_2 frame relative to g_1-frame
ω = inertial angular velocities along body coordinates, natural frequencies
ζ_{AB} = position of point A in coordinate system B
ψ_{rel} = payload roll angle relative to lateral gimbal

Superscripts

T = transpose of a matrix or vector
-1 = inverse
$\dot{}$, $\ddot{}$ = variable's first and second time derivatives (set above variable)

Introduction

DURING the extended space shuttle orbital missions of the 1980s, a number of solar-, stellar-, and Earth-viewing scientific experiments shall be performed. These experiments will require a highly accurate instrument pointing system for providing fine pointing in the presence of crew motion and other disturbances. With this objective in mind, a concept for such an apparatus, an annular suspension and pointing system (ASPS), was introduced.[1]

The annular suspension and pointing system (ASPS) includes two assemblies with connecting interfaces, each assembly having a separate function (see Fig. 1). The first assembly is attached to the carrier vehicle and consists of an elevation gimbal and a lateral gimbal which provide "coarse" pointing of the payload instrument by allowing two rotations of the instrument relative to the carrier vehicle. The second, or vernier, pointing assembly is made up of magnetic actuators for suspension and fine pointing, roll motor segments, and an instrument mounting plate around which a continuous annular rim (Fig. 2) is attached that provides appropriate magnetic circuits for the actuators and the roll motor segments. The payload assembly, consisting of the payload instruments, the mounting surface, and the annular rim, is suspended in the lateral coarse gimbal without physical contact and provides vernier attitude fine pointing and roll positioning of the instrument, as well as six-degree-of-freedom isolation from carrier motion disturbances. In addition, the second assembly has a rim-centering mode in which axial and radial rim position sensors located at each actuator station are used to center the rim axially and radially between actuator pole faces. This mode allows coarse gimbal slewing for retargeting, for Earth pointing, or for backup coarse gimbal pointing. Rubber guards are provided on the lateral gimbal in order to avoid accidental impact between rim and magnetic actuator pole faces.

Nominal operation of the ASPS for solar or stellar pointing first involves coarse gimbal pointing with coarse (wide field of view) sensors onboard the ASPS (or with sensors onboard vehicle and relative gimbal angle information). The rim-centering mode is activated during gimbal slewing. After coarse alignment, coarse roll positioning is accomplished by means of the rim roll motor and a relative roll sensor located on the rim, together with a carrier sensor or a sensor onboard the ASPS. After coarse attitude alignment, vernier fine pointing is initiated. For this mode, errors obtained from fine (narrow field of view) attitude sensors located on the ASPS (possibly a part of the payload instrument) are nulled by small magnetic suspension and fine pointing actuator torques applied to the annular rim. Also, translation rim centering is accomplished for this mode.

Nominal operation of the ASPS for Earth pointing initially involves establishing the correct elevation, lateral and roll attitudes, and attitude rates (slewing) in the rim-centering mode. After appropriate smooth instrument slewing is established, vernier pointing (similar to that described for solar and stellar pointing) is accomplished.

In this paper, a linearized mathematical model of the ASPS/space shuttle orbiter is derived. Control systems are designed for the magnetic actuators as well as the coarse gimbal torquers, so that the gimbals can automatically and continuously follow the payload (or vernier) assembly. Since the pointing performance is critically dependent on the payload attitude measurement system, payload attitude state estimators are designed for inclusion in the control loops. rms pointing performance in the presence of sensor and actuator noise and crew motion disturbance is evaluated by solving the covariance equation.

Mathematical Model Development

Coordinate Systems

(X_i, Y_i, Z_i) is an inertial system centered at 0_i. (X_s, Y_s, Z_s) is a shuttle-fixed system, centered at 0_s, the shuttle center of mass (Fig. 3). 0_s nominally coincides with 0_i. The Y_s axis is the longitudinal axis of the space shuttle as shown in Fig. 1. $(X_{g_1}, Y_{g_1}, Z_{g_1})$ is a coordinate system fixed to the elevation coarse gimbal, centered at P_1, and is obtained by one rotation ϕ_g about X_{g_1}. The axis X_{g_1} remains parallel to X_s. The coordinate system $(X_{g_2}, Y_{g_2}, Z_{g_2})$ is fixed to the lateral coarse gimbal; it is centered at P_2 and is obtained from the g_1 system by one rotation θ_g about Y_{g_2}. All the coordinate systems will hereafter be referred to by their subscripts, e.g., i, s, g_1, g_2, etc.

The inertial coordinate system (X_{il}, Y_{il}, Z_{il}) is also centered at 0_i, and is obtained by two rotations ϕ_I, θ_I (X, Y sequence) from the i system. ϕ_I and θ_I represent the target pointing angles relative to the i frame. The i_I system is used to express payload attitude.

The payload assembly consists of a cylindrical payload instrument, the instrument mounting surface, and the annular rim (Fig. 4). (X_p, Y_p, Z_p) is a coordinate system fixed to the payload assembly, centered at 0, its center of mass. The payload-fixed coordinate system (X_q, Y_q, Z_q) is parallel to (X_p, Y_p, Z_p) and is centered at point Q, which is the center of the instrument mounting surface.

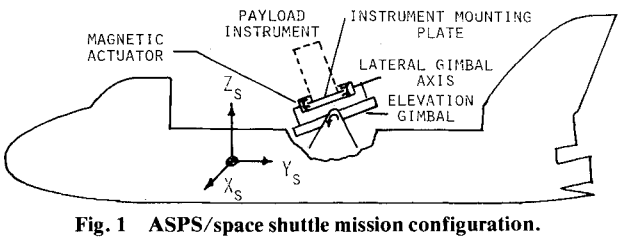

Fig. 1 ASPS/space shuttle mission configuration.

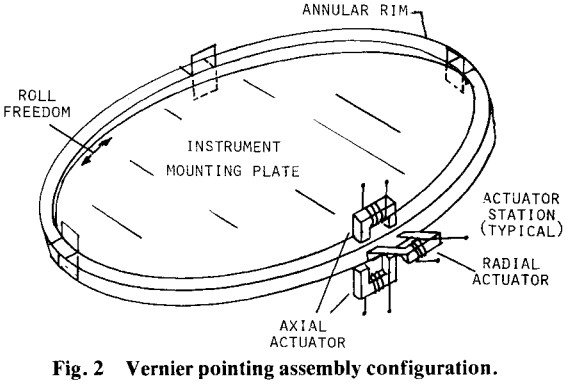

Fig. 2 Vernier pointing assembly configuration.

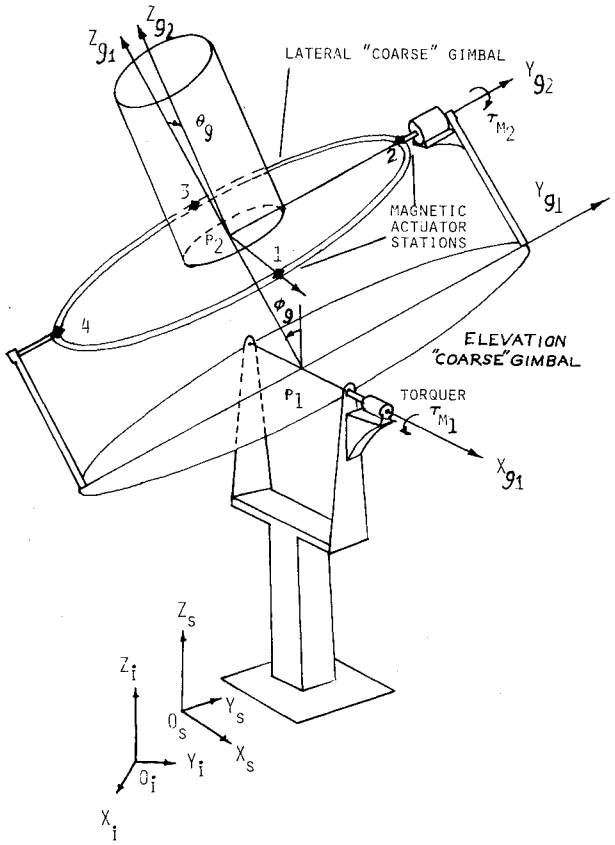

Fig. 3 Details of coarse pointing assembly.

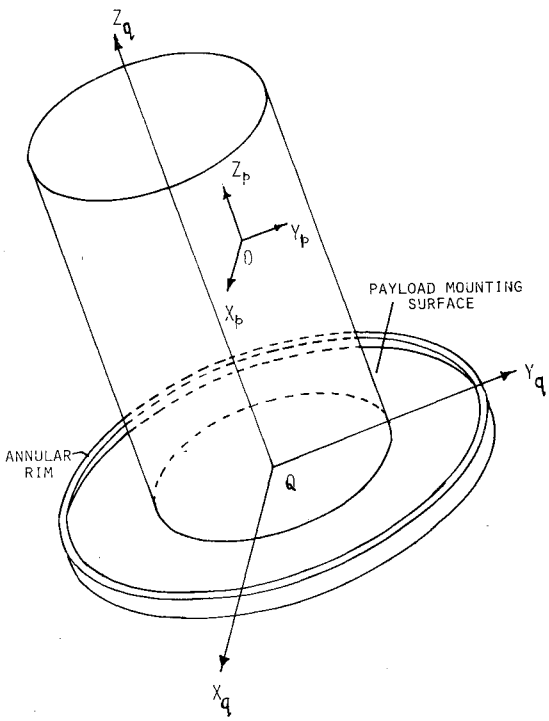

Fig. 4 Payload assembly.

The coordinate system (X_s, Y_s, Z_s) is obtained from (X_i, Y_i, Z_i) by a set of three rotations ϕ_s, θ_s, ψ_s in X, Y, Z sequence. The vector $\alpha_s = (\phi_s, \theta_s, \psi_s)^T$ thus defines the shuttle attitude. The payload system (X_p, Y_p, Z_p) is obtained from the i_1 system by a set of three rotations (X, Y, Z sequence) ϕ_p, θ_p, ψ_p. Thus the vector $\alpha_p = (\phi_p, \theta_p, \psi_p)^T$ defines the payload attitude.

Summary of Mathematical Model

The mathematical model is obtained via Lagrangian formulation. The complete system consists of two separate systems: 1) shuttle and coarse gimbals, and 2) payload assembly. Since these two systems are physically separated by magnetic actuator gaps, it was advantageous to derive separate models for each system and to interconnect them via magnetic actuator forces.

The coarse pointing assembly consists of three objects: shuttle, elevation gimbal, and lateral gimbal. Expressions are derived for the kinetic energies of the three objects in terms of the inertial velocities of their centers of mass, and their angular velocities relative to the inertial frame, expressed along the body coordinates of each object. The eight degrees of freedom are:

$$\zeta_{0_S i} = (X_{0_S i},\ Y_{0_S i},\ Z_{0_S i})^T,\ \alpha_s,\ \phi_g \quad \text{and} \quad \theta_g$$

The gimbal bearings are assumed to be frictionless. For the payload assembly, the six degrees of freedom are:

$$\alpha_p \quad \text{and} \quad \zeta_{0i_1} = (X_{0i_1},\ Y_{0i_1},\ Z_{0i_1})^T$$

Total degrees of freedom are fourteen; however, since only the position of the payload assembly relative to the coarse pointing assembly is of interest, three degrees of freedom are redundant. Thus, there are eleven minimal degrees of freedom.

The nonlinear equations of motion are given by:

$$\frac{\mathrm{d}}{\mathrm{d}t}\left(\frac{\partial T}{\partial \dot{q}_r}\right) - \frac{\partial T}{\partial q_r} = F_{q_r} \tag{1}$$

where T is the kinetic energy, q_r, $r=1,2,\ldots,n$, are the generalized coordinates, and F_{q_r} are the generalized forces. For the coarse assembly, linearization is performed about the equilibrium point

$$\zeta_{0_S i}(t) \equiv 0, \quad \alpha_s(t) \equiv 0, \quad \phi_g(t) \equiv \phi_l, \quad \theta_g(t) \equiv \theta_l$$

and the equations of motion are obtained in the following form:

Shuttle translation

$$A_{11}\ddot{\zeta}_{0_S i} + A_{12}\ddot{\alpha}_s + A_{13}\ddot{\phi}_g = F_{\zeta_{0_S i}} \tag{2}$$

Shuttle rotation

$$A_{21}\ddot{\zeta}_{0_S i} + A_{22}\ddot{\alpha}_s + A_{23}\ddot{\phi}_g + A_{24}\ddot{\theta}_g = F_{\alpha_s} \tag{3}$$

Elevation gimbal

$$A_{31}\ddot{\zeta}_{0_S i} + A_{32}\ddot{\alpha}_s + A_{33}\ddot{\phi}_g + A_{34}\ddot{\theta}_g = F_{\phi_g} \tag{4}$$

Lateral gimbal

$$A_{42}\ddot{\alpha}_s + A_{43}\ddot{\phi}_g + A_{44}\ddot{\theta}_g = F_{\theta_g} \tag{5}$$

In Eqs. (2-5), the symbols $\zeta_{0_S i}$, α_s, ϕ_g, θ_g denote their incremental values about the equilibrium point. A_{ij} are appropriately dimensioned coefficient matrices.

For the payload assembly, the linearized equations about $\alpha_q(t) \equiv 0$, $\zeta_{Qi_1}(t) \equiv 0$ are:

$$m_p(\ddot{\zeta}_{Qi_1} + H_{0q}\ddot{\alpha}_q) = F_{\zeta Qi_1} \tag{6}$$

where $H_{0q} = -Cp(\zeta_{0q})$

$$I_q\ddot{\alpha}_q + m_p H_{0q}{}^T\ddot{\zeta}_{Qi_1} = F_{\alpha q} \tag{7}$$

where the symbols α_q, ζ_{Qi_1} denote their incremental values about the equilibrium point. Substituting for $\ddot{\zeta}_{Qi}$ from Eq. (6) into Eq. (7),

$$(I_q - m_p H_{0q}{}^T H_{0q})\ddot{\alpha}_q = F_{\alpha q} - H_{0q}{}^T F_{\zeta qi_1} \tag{8}$$

But the moment of inertia of the payload assembly about the p axes is

$$I_p = I_q - m_p H_{0q}{}^T H_{0q}$$

Also, for the linearized system, $\alpha_q = \alpha_p$. Therefore, Eq. (8) becomes:

$$I_p \ddot{\alpha}_p = F_{\alpha q} - H_{0q}{}^T F_{\zeta Qi_1} \tag{9}$$

Considering position Eq. (2) for $\zeta_{0_s i}$, and position Eq. (6) for ζ_{Qi_1}, only the difference between the payload assembly position and the coarse pointing assembly is of interest. Define ϵ as

$$\epsilon = \zeta_{p_2 i_1} - \zeta_{Qi_1} \tag{10}$$

After linearization of the second derivative of this equation about the equilibrium point, simplification yields

$$\ddot{\zeta}_{0_s i} = D_{ii_1}^T(\ddot{\epsilon} + \ddot{\zeta}_{Qi_1}) - H_{p_2 s}\ddot{\alpha}_s - f(\zeta_{p_2 g_1})\ddot{\phi}_g \tag{11}$$

where $H_{p_2 s} = -C_p(\zeta_{p_2 s})$, and $f(\zeta_{p_2 g_1})$ is a linear function of $\zeta_{p_2 g_1}$. This value of $\ddot{\zeta}_{0_s i}$ is substituted into Eqs. (2-4) to obtain the equations for shuttle and gimbals in the following form:

$$[A]_{8\times 8}(\ddot{\epsilon}^T, \ddot{\alpha}_s^T, \ddot{\phi}_g, \ddot{\theta}_g)^T = [B]_{8\times 1} \tag{12}$$

The equation of motion for payload assembly is:

$$I_p \ddot{\alpha}_p = \sum_{j=1}^{4} C_p(\zeta_{Ajq} - \zeta_{0q}) F_j \tag{13}$$

Equations (12) and (13) define the complete linearized motion of the system.

Cable Forces and Torques

Flexible cables for data transmission and power supply are assumed to be routed through the lateral coarse gimbal and the center of the instrument mounting surface of the payload assembly. The cables are assumed to cause a constant axial force, a constant radial force, and a constant torque about the roll axis, as well as axial and radial spring forces (proportional to relative displacements) and torsion torque (proportional to relative roll angle).

This simple representation is used in order to keep the number of state variables small, and is considered to be adequate for the purpose of linear analysis. In the actual hardware, it is expected that cables can be avoided by using an optical data coupler and a battery pack on the vernier assembly; however, this model is included for the sake of completeness. In the linearized model, the cable torque exerted on the payload assembly is given by

$$T_{\text{cable}}^T = (0, 0, \quad T_b + K_{TS}\psi_{\text{rel}}) \tag{14}$$

$$F_{\text{cable}}^T = F_b^T + (K_{Fxs}\epsilon_x, K_{Fys}\epsilon_y, K_{Fzs}\epsilon_z) \tag{15}$$

Equal and opposite reactive forces and torques are also acting on the coarse pointing system. In the linear model, these additional terms can be easily included in the generalized force expressions to yield complete equations of uncontrolled motion.

Sensor Models

Measurements of shuttle attitude and attitude rate, contaminated with zero-mean white noise, are assumed to be available for synthesizing the shuttle attitude control inputs using such devices as Control Moment Gyros (CMG) or Annular Momentum Control Device (AMCD). It should be noted that this assumption about shuttle attitude controller is not critical, since the payload is almost completely isolated from the shuttle. This assumption is made only to facilitate linear analysis. Coarse gimbal rates $\dot{\phi}_g$ and $\dot{\theta}_g$ are measured by tachometers. These measurements are also contaminated with zero-mean white noise. The payload attitude measurement system consists of three rate gyros for measuring $\dot{\phi}_p$, $\dot{\theta}_p$, and $\dot{\psi}_p$, and two star trackers, one for measuring the pointing errors ϕ_p and θ_p, and the other, pointing away from the line of sight, for measuring roll angle error ψ_p. Each rate gyro output is contaminated with a colored noise and a Wiener process bias. The star trackers are inherently discrete time devices. The star tracker outputs are contaminated with uncorrelated time sequences. A bias may also be present in the tracker output. Gyro drift rate or bias, star tracker bias, and tracker boresight misalignment are important sources of error affecting pointing error. Gyro drift rate is estimated by a state estimator which gives asymptotically unbiased rate estimate. Star tracker bias errors are usually measurable and can be compensated to a large extent by the tracker electronics. Any uncompensated bias and misalignment will affect the mean, but not the standard deviation of pointing error. In pointing performance evaluation, the mean is sometimes called "pointing accuracy" and the standard deviation is called "pointing stability." In most missions the "accuracy" requirements are not very stringent; therefore, small tracker bias and misalignment errors can be tolerated and are assumed to be absent in this paper. A description of the payload attitude measurement system is given in Fig. 5.

The axial and radial rim-centering errors are measured by eight proximity sensors, two at each magnetic actuator station. The proximity sensor outputs are also contaminated with white noise. Thus, the complete measurement vector can be written as:

$$y^T = [\delta_1(x), \delta_1(z), \delta_2(y), \delta_2(z), \delta_3(x), \delta_3(z), \delta_4(y), \delta_4(z), \dot{\phi}_g, \dot{\theta}_g, \alpha_p, \dot{\alpha}_p, \alpha_s, \dot{\alpha}_s] + \text{additive noise} \tag{16}$$

where $\delta_i(j)$ denotes the centering error at the ith magnetic actuator station along j axis, $i = 1,2,3,4$; $j = x, y, z$.

Proximity Sensor Outputs

Axial and radial rim position sensors are located at each magnetic actuator station. In order to compute the magnetic

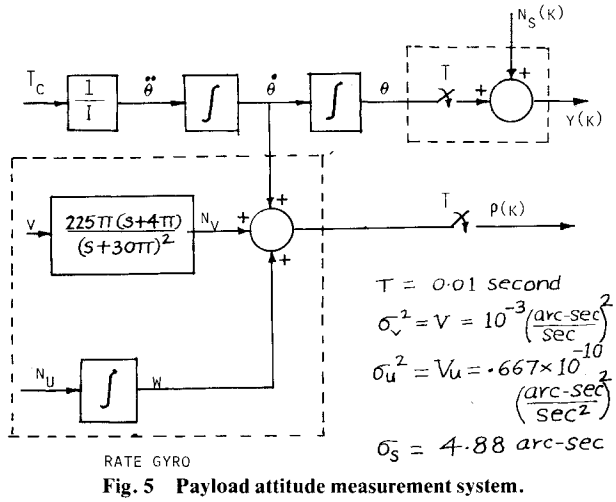

Fig. 5 Payload attitude measurement system.

actuator forces it is necessary to compute the centering errors at each actuator station. After linearization and simplification, the following expressions for the sensor outputs are obtained (excluding noise terms)

$$\delta_1(x) = \delta_3(x) = \epsilon_x \tag{17}$$

$$\delta_2(y) = \delta_4(y) = \epsilon_y \tag{18}$$

$$\delta_1(z) = \epsilon_z - r(\cos\phi_1\theta_s + \sin\phi_1\psi_s) - r(\theta_g - \theta_p) \tag{19}$$

$$\delta_2(z) = \epsilon_z + r(\cos\theta_1\phi_s + \sin\theta_1 \sin\phi_1\theta_s - \sin\theta_1\cos\phi_1\psi_s) + r(\phi_g\cos\theta_1 - \phi_p) \tag{20}$$

$\delta_3(z)$ and $\delta_4(z)$ are obtained from $\delta_1(z)$ and $\delta_2(z)$ by changing the sign of r.

Payload Attitude State Estimator Design

Pointing performance of space experiment pointing systems is critically dependent on the pointing error and error rate signals used for synthesizing the control laws. As mentioned earlier, for stellar pointing missions the pointing errors (vernier assembly or payload attitude angles) are assumed to be measured by two star trackers – one for ϕ_p and θ_p, and the other pointing at about right angles to z_q axis for ψ_p. For the purpose of this paper, it is assumed that the star tracker noises in ϕ_p and θ_p measurements are uncorrelated. It can be shown that direct use of noisy payload attitude and rate measurements will result in an unsatisfactory performance unless the noise levels are extremely low. Therefore, an estimator is needed in the loop. Two types of payload attitude state estimators are considered in this paper (one estimator is used per axis). Estimator I, due to Farrenkopf,[2] does not utilize the information about control torques applied to the payload. This estimator is very general, and uses the star tracker output as the only "observation." Referring to Fig. 5, however, both star tracker and rate gyro outputs can be treated as "observations" and a Kalman filter can be designed if the input torque is known. Since the ASPS uses magnetic actuators to generate control torques, the latter can be measured very accurately. A Kalman filter can therefore be designed in the usual manner.[3] This is termed Estimator II in this paper. By performing extensive computer simulations, it was shown[4] that star tracker output can be treated as continuous time (with noise variance appropriately modified as in Ref. 5) without significant loss of accuracy. All computations were therefore performed for continuous system. Estimator design is treated in Ref. 4 in detail. Estimators I and II in this paper refer to filters 1 and 3 designed in Ref. 4. Both of these estimators give asymptotically unbiased estimates of payload attitude and rate.

Control Systems Design

The three control systems to be considered are: coarse gimbal control systems, magnetic actuator control systems, and space shuttle attitude control system. The function of the coarse gimbal control system is to drive the two gimbal torque motors in such a way as to keep the rim centered within the magnetic actuators; that is, coarse gimbals follow the payload assembly while tracking a moving target. The coarse gimbal control system utilizes proximity sensor and gimbal rate tachometer outputs. The magnetic actuator control system is required to generate actuator forces for two purposes: to eliminate the rim-center position error ϵ, and to keep the payload assembly properly pointed at the target. The magnetic actuator control system utilizes payload attitude and rate estimates and proximity sensor outputs. The space shuttle attitude control system utilizes the attitude and attitude rate estimates to generate controlling torques. Control systems are designed assuming complete statistical separation; that is, they are designed assuming availability of noise-free sensor outputs. In the covariance analysis, however, sensor noise and payload attitude state estimators are included. Because of the presence of bias forces and torques due to cable, integrators must be used to eliminate steady-state error in ϵ. The bias error in payload attitude was found to be small (less than 0.15 arc-s in preliminary computation); therefore, no integrator is used in payload attitude control loop.

The control system design is accomplished by considering the desired response characteristics. Since the number of control variables is large, the desired response characteristics can be achieved in a straightforward manner, and the use of such tools as linear regulator theory is not necessary. In fact, a design based on linear regulator theory would be undesirable since it would require the feedback (estimates) of all the state variables.

Coarse Gimbal Control Systems

The coarse gimbal assembly, which consists of the elevation and lateral coarse gimbals, must automatically follow the payload assembly. This is assumed to be accomplished by the use of two brushless DC torquers. The objective of the control systems for the torquers is to move the coarse gimbals in such a manner that the payload assembly is kept properly centered in the magnetic bearings. Thus, an appropriate design approach is to obtain the command values of ϕ_g and θ_g which will minimize

$$J = \delta_1^2(x) + \delta_3^2(x) + \delta_2^2(y) + \delta_4^2(y) + \sum_{j=1}^{4} \delta_j^2(z) \tag{21}$$

This is done by substituting for δ_j from Eqs. (17-20), and for ϵ from Eq. (11), and making

$$\frac{\partial J}{\partial \phi_g} = \frac{\partial J}{\partial \theta_g} = 0$$

The solution gives the following command signals:

$$\phi_{gc} - \phi_g = \frac{1}{z_{P_2g_1}^2 + r^2\cos^2\theta_1}\left[z_{P_2g_1}\delta_2(y) - \frac{r\cos\theta_1}{2} \times \{\delta_2(z) - \delta_4(z)\}\right] \tag{22}$$

where $\zeta_{P_2g_1} = (0, 0, z_{P_2g_1})^T$

and

$$\theta_{gc} - \theta_g = \frac{\delta_1(z) - \delta_3(z)}{2r} \tag{23}$$

The torques to be generated by the coarse gimbal torquers are then given by

$$\tau_{m_1} = -K_{g_1}\dot{\phi}_g + L_{g_1}(\phi_{gc} - \phi_g) \tag{24}$$

$$\tau_{m_2} = -K_{g_2}\dot{\theta}_g + L_{g_2}(\theta_{gc} - \theta_g) \tag{25}$$

where K_{g_1} and K_{g_2} are rate gains, and L_{g_1} and L_{g_2} are proportional gains. The desired response can be obtained (approximately) by making

$$K_{gi} = 2\rho_{gi}\omega_{gi}I_{gi}, \quad L_{gi} = \omega_{gi}^2 I_{gi}, \quad i = 1,2 \tag{26}$$

where I_{gi} is the appropriate axis inertia.

Magnetic Actuator Control Systems

Magnetic actuators serve a dual purpose: they keep the rim center properly positioned within the lateral coarse gimbal, and they keep the payload properly pointed at the target. The

desired control is achieved by generating appropriate magnetic forces acting (nominally) along x_q, y_q, z_q directions at each of the four actuator stations. Thus there are 12 control forces. Ignoring the rotation-translation coupling, the desired responses can be obtained by making

$$\begin{bmatrix} \sum_{j=1}^{4} F_{xj} \\ \sum_{j=1}^{4} F_{yj} \\ \sum_{j=1}^{4} F_{zj} \end{bmatrix} = m_{10}\lambda_{\vartheta} \tag{27}$$

and

$$C_{\zeta 0}\sum_{j=1}^{4} F_j - rf = -I_{p0}\lambda_{\alpha p} \tag{28}$$

where

$$f = (F_{z_4} - F_{z_2},\quad F_{z_1} - F_{z_3},\quad F_{x_2} - F_{x_4} + F_{y_3} - F_{y_1})^T \tag{29a}$$

$$m_1 = mm_p/(m+m_p),\quad C_{\zeta} = -C_p(\zeta_{0q}) \tag{29b}$$

The subscript *0* implies the measured or estimated value of the parameter. The terms $\lambda_{\epsilon} = (\lambda_{\epsilon x}, \lambda_{\epsilon y}, \lambda_{\epsilon z})^T$, and $\lambda_{\alpha p} = (\lambda_{\phi p}, \lambda_{\theta p}, \lambda_{\psi p})^T$ represent the desired accelerations, that is,

$$\lambda_{\epsilon x} = 2\rho_x\omega_x\dot{\epsilon}_x + \omega_x^2\epsilon_x + z_{IX} \tag{30}$$

and so forth, where

$$\dot{z}_{IX} = C_{IX}\epsilon_x \tag{31}$$

The first two terms in the right-hand side of Eq. (30) represent appropriate decay characteristics, while the last term is the integral term [Eq. (31)] added in order to eliminate steady-state position errors because of cable bias forces. Since no integrators are used in the payload attitude control loop,

$$\lambda_{\phi p} = 2\rho_{\phi p}\omega_{\phi p}\dot{\phi}_p + \omega_{\phi p}^2\phi_p \tag{32}$$

and so forth.

Defining

$$a_x = 2\rho_x\omega_x,\quad b_x = \omega_x^2,\quad a_{\phi p} = 2\rho_{\phi p}\omega_{\phi p},\quad b_{\phi p} = \omega_{\phi p}^2$$

and so forth, one can readily determine position, rate, and integral (for the ϵ loop) gains from desired natural frequencies and damping ratios. Because of cable spring constants in the ϵ loop, the effective proportional gain is approximately given by

$$b_{xe} = b_x + (K_{sx}/m_p)$$

This must be taken into account while determining gains which give desired decay characteristics for ϵ. Thus the control force equation can be written in the following matrix-vector form:

$$A_{CF}F = q$$

where

$$F = (F_{x_1}, F_{x_2}, F_{x_3}, F_{x_4}, F_{y_1}, F_{y_2}, F_{y_3}, F_{y_4}, F_{z_1}, F_{z_2}, F_{z_3}, F_{z_4})^T \tag{33}$$

$$q = [m_{10}\lambda^T\epsilon, (1/r)(I_{p0}\lambda_{\alpha p} + C_{\zeta 0}m_{10}\lambda_{\epsilon})^T]^T \tag{34}$$

A_{CF} = appropriate 6×12 coefficient matrix.

Letting

$$F_{x_1} = F_{x_3} = \tfrac{1}{2}m_{10}e_1^T\lambda_{\epsilon} \tag{35a}$$

$$F_{y_2} = F_{y_4} = \tfrac{1}{2}m_{10}e_2^T\lambda_{\epsilon} \tag{35b}$$

the remaining equations are in the form:

$$A'_{CF}F' = q'$$

where

$$F' = (F_{x_2}, F_{x_4}, F_{y_1}, F_{y_3}, F_{z_1}, F_{z_2}, F_{z_3}, F_{z_4})^T$$

$$q' = q - (F_{x_1} + F_{x_3}, F_{y_2} + F_{y_4}, 0, 0, 0, 0)^T$$

The solution which minimizes the norm of F' is given by

$$F' = (A'_{CF})^T[A'_{CF}(A'_{CF})^T]^{-1}q'$$

which, after simplification, gives F' as a function of ϵ, $\dot{\epsilon}$, α_p, and $\dot{\alpha}_p$. This design gives complete payload isolation from the coarse assembly if payload inertia and position of center of mass are known accurately.

Implementation

Proximity sensors provide noisy measurements of the radial and axial errors. In order to generate proportional and rate signals required for the ϵ loop, three second-order filters of the following type are used:

$$G_{\epsilon x}(s) = \frac{a_x s + b_x}{c_1 s^2 + c_2 s + 1} = \frac{Y_{\epsilon x}(s)}{\epsilon_x(s)} \tag{36}$$

This network can effectively generate proportional and rate signals with low noise level. A first-order filter would have resulted in infinite variance with white measurement noise because of its constant high-frequency gain. The integrator can be implemented as in Eq. (34) without the necessity of a filter. The signals ϵ_x, ϵ_y, ϵ_z used in implementation are obtained from the noisy proximity sensor outputs of Eqs. (17-20). For α_p loop, the attitude and rate signals [used in Eq. (32)] are obtained from the state estimator.

Space Shuttle Attitude Control System

Attitude of the space shuttle is assumed to be controlled by such devices as CMG's or AMCD, which generate stabilizing torques using white noise-contaminated attitude and attitude rate signals. This assumption facilitates linear analysis and is not restrictive since the payload assembly is almost completely isolated from the space shuttle. Desired control torque is given by

$$T_{\text{cons}} = -I_s\lambda_{\alpha_s} \tag{37}$$

where

$$\lambda_{\alpha_s} = (\lambda_{\phi_s}, \lambda_{\theta_s}, \lambda_{\psi_s})^T \tag{38}$$

$$\lambda_{\phi_s} = 2\rho_{\phi_s}\omega_{\phi_s}\dot{\phi}_s + \omega_{\phi_s}^2\phi_s,\quad \text{etc.} \tag{39}$$

Attitude and rate measurements are contaminated with white noise. Thus the controller is required to generate large control torques [Eq. (51)] proportional to the additive noise. In order to avoid this, and to reflect controller bandwidth, first-order filters are used to filter the noisy signals λ_{ϕ_s}, λ_{θ_s}, and λ_{ψ_s}.

Equations of Motion of the Controlled System

Crew-Motion Models

The space shuttle is excited by force and moment inputs generated by the movement of the crew members at the crew

station. The crew motion forces and moments can be approximated by zero-mean band-limited white noise processes.[6]

Each crew-motion force or moment is generated by passing a unit power spectral density white noise process through a linear filter represented by the general transfer function

$$H(s) = \frac{\tau_{c_1} s(\tau_{C_2} s + 1)}{(s^2 + 2\rho_1\omega_1 s + \omega_1^2)(s^2 + 2\rho_2\omega_2 s + \omega_2^2)} \tag{40}$$

Therefore, a total of six filters, three for forces and three for moments, are required to describe each crew activity. State-space equations for the crew motion model can be written as[1]

$$\dot{x}_c = A_{\rm cr} x_c + b_{\rm cr} u_c \tag{41}$$

$$v_c = (F_c^T,\ T_c^T)^T = T_{\rm cr} x_c \tag{42}$$

where x_c is the n_f-dimensional state vector, u_c is unity power spectral density white noise, v_c is 6×1 force and moment vector, $A_{\rm cr}$, $b_{\rm cr}$, $T_{\rm cr}$ are $n_f \times n_f$, $n_f \times 1$, and $6 \times n_f$ matrices.

Complete Closed-Loop Equations

Complete closed-loop equations consist of equations of motion for the space shuttle/ASPS and controllers, crew motion filters, payload attitude state estimators, filters used in ϵ loops and α_s loops, and integrators used to offset steady-state errors in ϵ. As mentioned earlier, star tracker outputs can be accurately represented as continuous time signals after appropriate modification of their noise variances. Therefore, the complete system can be represented by

$$\dot{x} = Ax + Bw_T + w_{\rm bias}$$

where x is the total state vector and w_T is the total noise vector containing all input and measurement noise terms. $w_{\rm bias}$ is a bias vector which appears because of cable forces and torques.

Method of Solution

Pointing performance of the system is represented by 1) pointing accuracy, or bias, or mean, and 2) pointing stability, or standard deviation about the mean. The steady-state bias in state vector x, denoted by x_b, can be readily obtained as

$$x_b = -A^{-1} w_{\rm bias} \tag{43}$$

Vector x_b thus contains information about the pointing accuracy.

Covariance matrix Σ of state vector about the mean evolves according to the equation[5]

$$\dot{\Sigma} = A\Sigma + \Sigma A^T + BW_T B^T \tag{44}$$

where

$$\Sigma(t) = E\{[x(t) - x_b][x(t) - x_b]^T\}$$

and W_T is the covariance intensity matrix of w_T. This is a linear matrix equation of order n, where $n = 34 + n_e + n_f$, n_e is the order of estimator state vector, and n_f is the order of the crew-motion filter. With Estimator I and for a typical crew activity, $n = 68$. The method of Ref. 7 was found to be satisfactory for obtaining solution Σ of the steady-state version of Eq. (44). This method has a provision for generating successive corrections in order to get highly accurate solutions.

Numerical Results and Discussion

In order to investigate pointing performance of the ASPS, two different payloads were selected. Payload 1, which has a mass of 270 kg, is 3.7 m long and 0.66 m in diameter, and is representative of relatively small stellar observation payloads. Payload 2, which has a mass of 4857 kg, is 3.35 m in diameter and 1.99 m long, and is representative of large payloads such as those containing X-ray equipment. Parameters of space shuttle and the payloads are given in Tables 1a-1c. The only physical contact between the payload and the coarse gimbals is a data transmission/power supply cable which is routed through the center of the instrument mounting plate. Bias forces and torques, and spring constants due to cable are given in Table 1d. For the present computation, all the radial bias force is assumed to be acting in the X_q direction. Parameters of space shuttle attitude control system, coarse gimbal control systems, magnetic actuator control systems, and various filters used in the system are given in Table 2. Nominal values of standard deviations of all white noise sources are given in Table 3. In order to make the analysis as realistic as possible, it was assumed that an error exists in the measurements of payload mass, inertia matrix, and center of mass location. To keep the number of variables small, the same per-unit error δ was assumed to be made in measuring m_p, I_p, and ζ_{0q}.

Preliminary computations indicated that the current star tracker/rate gyro package (described in Fig. 5) is the most important source of error. The rms pointing error due to star tracker/rate gyro uncertainties with Estimator I (Filter 1A of Ref. 4) is about 0.125 arc-s along each axis. This is sufficiently large to obscure the effect of all other sources of error, including crew motion. However, with the availability of better attitude measurement packages and better estimation schemes, such as Estimator II (Filter 3 of Ref. 4), other sources of error can become important. It is therefore important to investigate the sensitivity of rms pointing error to various sources of noise, when perfect payload attitude and rate measurements are available. In order to do this, the attitude measurement and estimation system was removed along with star tracker/rate gyro uncertainties and each source of error (e.g., crew motion, proximity sensor noise, shuttle attitude measurement noise, coarse gimbal tachometer noise) was individually activated. The target pointing angles were: $\phi_l = 45$ deg, $\theta_l = 45$ deg, which were determined earlier to form one of the worst combinations. Error parameter δ was at its worst case value of 0.1. The crew activity considered in this report is "shower" because of its reported severity.[1] Table 4a shows the sensitivity results for both payloads. It was found that the rms pointing error is relatively insensitive to proximity sensor noise, but is significantly sensitive to shuttle attitude measurement noise. This is because white shuttle attitude and rate measurement noise enters the system under the present assumption. In the actual system, however, shuttle attitude is controlled by reaction control jets and white noise does not enter the system. Shuttle-to-payload coupling exists only through cable spring constants and non-zero error parameter δ. To investigate the extent to which cables affect the sensitivities, δ was made zero and the sensitivities were

Table 1a Space shuttle orbiter parameters

Mass, kg	86176.2
Inertias, (kg-m^2)	
I_{xx}	7,882,725
I_{yy}	1,037,200
I_{zz}	8,082,030
I_{xy}	6,779
I_{xz}	2,711
I_{yz}	−178,968
Crew station location (s-system, m)	(0, −16.002, 0.594)
Location of P_l (s-system, m)	(0, 2.2, 0.75)

Table 1b Payload parameters

	Mass, kg	Length, m	Diameter, m	r, m	Inertias, kg-m^2 I_{xx}	I_{yy}	I_{zz}
Payload 1	270	3.7	0.66	0.608	319.5	319.5	15.22
Payload 2	4857	1.99	3.35	1.98	5160	5160	6830
c.m. location in q-system:	Payload 1, m (.0508, .0508, 1.83)						
	Payload 2, m (.305, .305, 1.22)						

Table 1c Coarse gimbal parameters

	Payload 1			Payload 2		
	Mass, kg	$I_{xx}(=I_{yy})$, kg-m^2	I_{zz}, kg-m^2	Mass, kg	$I_{xx}(=I_{yy})$, kg-m^2	I_{zz}, kg-m^2
Elevation gimbal	14.63	2.72	5.42	45.4	89.0	178
Lateral gimbal	11.48	2.12	4.24	45.4	89.0	178

Table 1d Cable forces and torques

Bias force	0.01405 N radial, .00445 N axial
Spring constant (translation)	1.05 N/m radial, 0.35 N/m axial
Bias torque about roll axis	0.001 N-m
Spring constant (rotation) about roll axis	0.005 N-m/rad

Table 2 Control system parameters

Control system	Damping ratio, ρ	Natural frequency, ω Nominal	Range
Shuttle attitude	0.5	0.5 rad/s	0.1 – 1 rad/s
Coarse gimbals	0.7	2 Hz	1 Hz – 4 Hz
Payload attitude	0.7	2 Hz	1 Hz – 4 Hz
Rim position	0.7	0.05 rad/s	0.005 – 0.1 rad/s

Table 3 Measurement noise

Source description	Number of measurements	Standard deviation
Proximity sensors, axial and radial	8	2.54×10^{-7} m
Tachometers (coarse gimbal rate measurements)	2	0.1 deg/s
Shuttle attitude	3	0.01 deg
Shuttle attitude rate	3	0.1 deg/s
Star-tracker	3[a]	4.88 arc-s
Rate gyro (rate noise)	3	0.0316 arc-s/s^2
Rate gyro (bias noise)	3	8.16×10^{-16} arc-s/s

[a] Assumed.

obtained for payload 2. The results are shown in Table 4b. Finally, in an attempt to arrive at a more realistic representation of shuttle attitude measurement noise, the white shuttle attitude and rate measurement noises were passed through first order filters of 0.1 rad/s bandwidth. The sensitivities computed for payload 2 are shown in Table 4c. Effect of shuttle attitude measurement noise was significantly reduced as a result of using band-limited noise. Sensitivities to other noise sources remain unchanged.

Star tracker/rate gyro models and Estimator I were next reinserted in the system. With nominal parameters for these models, covariance computations were performed for various pointing angles: $\phi_I = 0$, 45, and 60 deg; $\theta_I = 0$, 45, and 60 deg, for $\delta = -0.1$, 0, and 0.1. Table 5 shows the rms errors obtained for payloads 1 and 2 for the worst case.

In order to determine the performance with a better star tracker/rate gyro package, star tracker noise standard deviation σ_s and rate gyro noise standard deviation σ_v were reduced by a factor of 10. Kalman filters (Estimator I) were designed for each axis. The resulting pointing performances are given in Table 6 for the two payloads. For all the cases considered, the magnetic actuator centering errors remained within 0.4 mm rms. It is expected that the use of Estimator II can yield much superior pointing performance if the input noise is small. Although model for input noise was not available, Estimator II (one for each axis) was designed for input noise $\sigma_{in} = 1\times10^{-6}$. These estimators were inserted in the loop and covariance computations were performed. The results are shown in Table 7 for payloads 1 and 2 with all noise parameters held at their nominal values, and $\delta = 0.1$. Estimator II yields maximum per axis rms pointing error of about 0.026 arc-s. This value, however, will be largely dependent on σ_{in}; therefore, more meaningful results with

Table 4a Sensitivities and bias due to cable

Source	Payload 1, arc-s, rms ϕ_p	θ_p	ψ_p	Payload 2 arc-s, rms ϕ_p	θ_p	ψ_p
Proximity sensors	3.58×10^{-6}	3.12×10^{-6}	2.77×10^{-6}	1.59×10^{-5}	1.53×10^{-5}	4.13×10^{-7}
Tachometer	1.87×10^{-3}	2.95×10^{-8}	1.09×10^{-3}	8.3×10^{-4}	4.01×10^{-7}	1.52×10^{-4}
Shuttle attitude and rate	5.26×10^{-4}	6.99×10^{-3}	4.17×10^{-3}	7.45×10^{-4}	2.74×10^{-3}	6.52×10^{-4}
Crew motion	4.31×10^{-4}	7.44×10^{-4}	5.54×10^{-4}	5.13×10^{-4}	2.46×10^{-4}	1.23×10^{-4}
All together	1.99×10^{-3}	7.03×10^{-3}	4.34×10^{-3}	1.23×10^{-3}	2.75×10^{-3}	6.82×10^{-4}
Bias error due to cable	1.02×10^{-2}	1.15×10^{-1}	-1.46×10^{-1}	3.8×10^{-4}	4.41×10^{-3}	-1.08×10^{-3}

Table 4b Sensitivities with $\delta = 0$

Source	Payload 2, arc-s, rms ϕ_p	θ_p	ψ_p
Proximity sensors	2.45×10^{-11}	4.16×10^{-10}	7.88×10^{-11}
Tachometer	1.01×10^{-10}	1.61×10^{-9}	3.16×10^{-10}
Shuttle attitude and rate	1.27×10^{-5}	1.52×10^{-4}	2.89×10^{-5}
Crew motion	1.11×10^{-6}	1.66×10^{-5}	3.03×10^{-6}
All together	1.28×10^{-5}	1.53×10^{-4}	2.91×10^{-5}

Table 4c Sensitivities with bandlimited shuttle attitude and rate noise

Noise source	ϕ_p	θ_p	ψ_p
Shuttle attitude and rate	1.38×10^{-4}	5.14×10^{-4}	1.22×10^{-4}
All together	9.85×10^{-4}	5.72×10^{-4}	2.33×10^{-4}

Table 5 rms errors with Estimator I

	rms error, arc-s σ_{ϕ_p}	σ_{θ_p}	σ_{ψ_p}
Payload 1	0.1252	0.1254	0.1253
Payload 2	0.1252	0.1252	0.1252

Table 6 rms errors for lower star-tracker and rate gyro uncertainties (Estimator I), arc-s

	σ_{ϕ_p}	σ_{θ_p}	σ_{ψ_p}
Payload 1	0.1285×10^{-1}	0.147×10^{-1}	0.1366×10^{-1}
Payload 2	0.1278×10^{-1}	0.1304×10^{-1}	0.1275×10^{-1}

Table 7 rms errors with Estimator II, arc-s

	σ_{ϕ_p}	σ_{θ_p}	σ_{ψ_p}
Payload 1	0.0234	0.0257	0.0242
Payload 2	0.0229	0.0241	0.0231

Estimator II can be obtained only after σ_{in} has been exactly determined from physical considerations.

Conclusions

A linear mathematical model has been developed for the space shuttle/ASPS which takes into account all internal couplings. Control laws and payload attitude state estimators have been designed in order to obtain satisfactory performance. The star tracker/rate gyro package used for payload attitude and rate measurement is the most significant source of error. The worst case pointing error was about 0.125 arc-s rms for each axis with the given star tracker/rate gyro package. With star tracker and rate gyro uncertainties reduced by a factor of 10, the worst case rms pointing error was about 0.013 arc-s for each axis. These results were obtained using Estimator I. It was found that it is possible to improve the pointing performance considerably by using a better payload attitude state estimator (Estimator II) if the input noise is low. It is concluded on the basis of this study that the ASPS offers a highly accurate auxiliary instrument pointing system and holds the promise for significant further improvement in its pointing performance.

Acknowledgment

This work was performed at NASA Langley Research Center under grant NSG-1241. The author would like to express his sincere gratitude to W.W. Anderson, N.J. Groom, and C.R. Keckler of LaRC for several very useful discussions.

References

[1] Anderson, W.W. and Joshi, S.M., *The Annular Suspension and Pointing (ASP) System for Space Experiments and Predicted Pointing Accuracies,* NASA TR R-448, 1975.

[2] Farrenkopf, R.L., "Generalized Results for Precision Attitude Reference Systems Using Gyros," *Proceedings of the AIAA Conference on Mechanics and Control of Flight,* Anaheim, Calif., Aug. 1974.

[3] Jazwinski, A.H., *Stochastic Processes and Filtering Theory,* Academic Press, New York, 1970.

[4] Joshi, S.M., "Analysis of Pointing Performance Limits of Space Experiment Pointing Systems in the Presence of Sensor and Actuator Noise, Old Dominion University Research Foundation, Technical Report 76-T3, March 1976.

[5] Kwakernaak, H. and Sivan, R., *Linear Optimal Control Systems,* Wiley-Interscience, New York, 1972, pp. 100, 470.

[6] Hendricks, T.C. and Johnson, C.H., "Stochastic Crew Motion Modeling," *Journal of Spacecraft and Rockets,* Vol. 8, Feb. 1971, pp. 150-154.

[7] Smith, P.G., "Numerical Solution of the Matrix Equation $AX+XA^T+B=0$," *IEEE Transactions on Automatic Control,* Vol. AC-16, June 1971, pp. 278-279.